Available online at www.sciencedirect.com

SciVerse ScienceDirect

Ceramics International 39 (2013) 5255–5262

CERAMICS INTERNATIONAL

www.elsevier.com/locate/ceramint

Synthesis and ethanol sensing properties of CuO nanorods coated with In_2O_3

Sunghoon Park[a], Hyunsung Ko[a], Soyeon An[a], Wan In Lee[b], Sangmin Lee[c], Chongmu Lee[a,*]

[a]Department of Materials Science and Engineering, Inha University, 253 Yonghyun-dong, Nam-gu, Incheon 402-751, Republic of Korea
[b]Department of Chemistry, Inha University, 253 Yonghyun-dong, Nam-gu, Incheon 402-751, Republic of Korea
[c]Department of Electronic Engineering, Inha University, 253 Yonghyun-dong, Nam-gu, Incheon 402-751, Republic of Korea

Received 21 November 2012; received in revised form 30 November 2012; accepted 8 December 2012
Available online 25 December 2012

Abstract

CuO/In_2O_3 core–shell nanorods were fabricated using thermal evaporation and radio frequency magnetron sputtering. X-ray diffraction and transmission electron microscopy showed that both the cores and shells were crystalline. The multiple networked CuO/In_2O_3 core–shell nanorod sensors showed responses of 382–804%, response times of 36–54 s and recovery times of 144–154 s at ethanol (C_2H_5OH) concentrations ranging from 50 to 250 ppm at 300 °C. These responses were 2.3–2.8 times higher than those of the pristine CuO nanorod sensor over the same C_2H_5OH concentration range. The origin of the enhanced ethanol sensing properties of the core–shell nanorod sensor is discussed.
© 2012 Elsevier Ltd and Techna Group S.r.l. All rights reserved.

Keywords: CuO nanorods; In_2O_3 shells; Gas sensors; Ethanol

1. Introduction

Cupric oxide (CuO) with a band gap of approximately 1.2–1.9 eV is one of the few metal oxides with p-type semiconducting properties [1,2]. These properties make CuO suitable for catalysis [3], lithium–copper oxide electrochemical cells [4], field emission device [5], gas sensors applications [6], high temperature superconductors [7], magnetic storage media [8], photovoltaics [9], infrared photodetectors, and heterogeneous catalysts [10]. A range of CuO nanostructures, such as nanoparticles, nanoribbons, plates and nanowires have been reported to be sensitive to humidity, HCOH, C_2H_5OH, NO_2, H_2S and CO [11–16]. One-dimensional (1D) CuO nanostructures have been synthesized using wet chemical methods, room-temperature liquid–solid growth, low-temperature solid-phase processes, or anodic aluminum oxide (AAO) template-assisted electrodeposition, liquid–liquid methods and catalyzed synthesis [17–24]. These methods have difficulty in controlling the diameters and composition of nanowires, and are unsuitable for mass production. On the other hand, CuO 1D nanostructures can also be synthesized on copper substrate using simple thermal oxidation processes [20].

In recent years, one-dimensional (1D) nanostructure-based sensors have become a subject of intense research effort because of the higher sensitivity, superior spatial resolution and rapid response associated with individual nanowires due to the high surface-to-volume ratios compared to thin film gas sensors [25–27]. Nevertheless, enhancing their sensing performance and detection limit is still a challenge. Core–shell 1D nanostructures has been fabricated to improve the sensitivity, stability and response speed of the 1D nanostructure-based sensors [28–30]. This paper reports the synthesis of CuO/In_2O_3 core–shell nanorods by the direct heating of Cu sheets in air followed by radio frequency (rf) magnetron sputtering of In_2O_3 as well as their enhanced ability to detect ethanol (C_2H_5OH) gas. The origin of the enhanced sensing properties of CuO/In_2O_3 core–shell nanorods is also discussed.

2. Experimental

The CuO/In_2O_3 core–shell nanorods were synthesized using thermal evaporation and sputtering methods. First,

*Corresponding author. Tel.: +82 32 860 7536; fax: +82 32 862 5546.
E-mail address: cmlee@inha.ac.kr (C. Lee).

0272-8842/$ - see front matter © 2012 Elsevier Ltd and Techna Group S.r.l. All rights reserved.
http://dx.doi.org/10.1016/j.ceramint.2012.12.026

the CuO nanorods were synthesized in a quartz tube furnace by the thermal oxidation of a copper sheet at 500 °C in air without a metal catalyst or the supplying of any other gas. The thermal oxidation process was carried out for 2 h and the furnace was cooled to room temperature. Subsequently, the CuO nanorods were coated with a thin In_2O_3 layer by conventional radio frequency (rf) magnetron sputtering. The base pressure, working pressure and Ar gas flow rate were 5.0×10^{-6} Torr, 2.0×10^{-2} Torr and 20 sccm, respectively. The rf sputtering power and sputtering time was 100 W and 10 min, respectively. The substrate temperature was maintained at room temperature.

Scanning electron microscopy (SEM, Hitachi S-4200), transmission electron microscopy (TEM, Philips CM-200), energy-dispersive X-ray spectroscopy (EDXS), and X-ray diffraction (XRD, Philips X'pert MRD diffractometer) were performed on the nanorod samples collected. The crystallographic structure was determined by glancing angle XRD using Cu K_α radiation (0.15406 nm) at a scan rate of 4°/min and at a glancing angle of 0.5° with a rotating detector.

The electrical and gas sensing properties of the plain and CuO/In_2O_3 core–shell nanorods were measured using a home-built computer-controlled characterization system consisting of a test chamber, sensor holder, Keithley sourcemeter-2612, mass flow controllers and data acquisition system. A given amount of ethanol (> 99.99%) gas was injected into the testing tube through a microsyringe, and the output resistance across the sensor was monitored. The resistance of the sensor in dry air or in a test gas was measured from this voltage.

The response of the CuO nanorod sensors was defined as R_a/R_g for C_2H_5OH, where R_a and R_g are the electrical resistances in the sensors in air and target gas, respectively. The response time is defined as the time needed for the change in electrical current to reach 90% of the equilibrium value after injecting the gas. The recovery time is defined as the time needed for the sensor to return to 90% of the original current in air after removing the gas.

3. Results and discussion

XRD was conducted to determine the crystal structure of the nanorods. The XRD pattern of CuO/In_2O_3 core–shell nanorods suggested that both CuO cores and In_2O_3 shells were crystalline (Fig. 1). Most XRD peaks of the core–shell nanorods were assigned to the planes of end-centered monoclinic-structured CuO with the following lattice constants: $a=0.4689$ nm, $b=0.3420$ nm, $c=0.5130$ nm and $\beta=99.57$ (JCPDS no. 89-5899). Only three tall peaks were assigned to the (111), (110), and (200) reflections of simple cubic structured-Cu_2O with a lattice constant of $a=0.4267$ nm (JCPDS no. 78-2076). Four peaks were assigned to the reflections of body-centered cubic (bcc)-structured In_2O_3 with lattice constants of $a=1.011$ nm (JCPDS no. 89-4595). The thermal oxidation of Cu in air converts the metal to Cu_2O first and then into

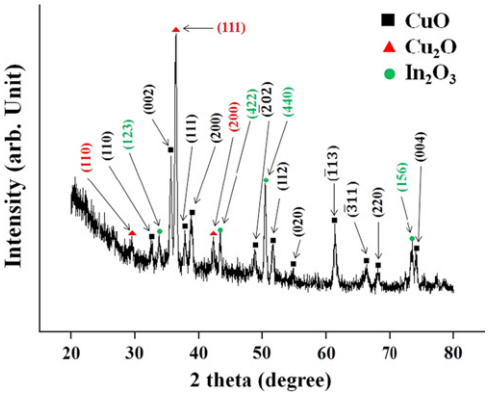

Fig. 1. XRD patterns of the CuO/In_2O_3 core–shell nanorods.

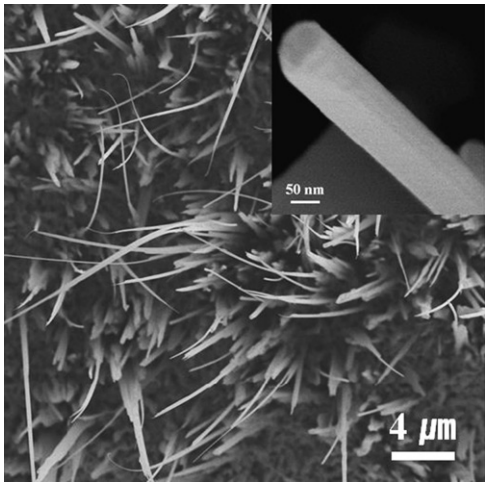

Fig. 2. SEM images of CuO/In_2O_3 core–shell nanorods. Inset, an enlarged SEM image of a typical core–shell nanorod.

CuO [22,31]:

$$4Cu + O_2 \rightarrow 2Cu_2O \quad (1)$$

$$2Cu_2O + O_2 \rightarrow 4CuO \quad (2)$$

CuO is known to form at ~270 °C. Nevertheless, XRD of the copper oxide nanorods synthesized by heating at 500 °C in air for 2 h showed the coexistence of both monoclinic CuO and simple cubic Cu_2O phases. Reaction (2) does not appear to have been complete, even at a high temperature of 500 °C.

Fig. 2 shows a SEM image of the CuO/In_2O_3 core–shell nanorods prepared by thermal oxidation followed by sputtering. Each 1D nanostructure exhibited a rod-like morphology as can be seen in the enlarged SEM image of a typical 1D nanostructure (inset in Fig. 2). SEM also showed that the synthesis scheme adopted in this study can grow CuO nanorods with diameters of 50–100 nm and lengths up to a few tens of micrometers. The low-magnification TEM image of a typical core–shell nanorod showed a CuO core with a diameter of ~80 nm at the central region and In_2O_3 shells at the two edge regions of

the nanorods with thicknesses of 5 nm and 15 nm (Fig. 3(a)). The high resolution TEM (HRTEM) image revealed fringe pattern both in the core and shell regions. The clear spotty patterns in the corresponding selected area electron diffraction (SAED) pattern was fitted to monoclinic structured-CuO (JCPDS no. 89-5899) (Fig. 3(c)). On the other hand, the dim spotty and concentric ring pattern was fitted to simple cubic Cu_2O with a lattice constant of $a=0.4267$ nm and bcc In_2O_3 with a lattice constant of $a=1.011$ nm (JCPDS no. 89-4595), respectively. The core in the core–shell nanorod contains both single crystal CuO and Cu_2O phases, while the shell contains polycrystalline In_2O_3 phase from the SAED pattern.

EDX of the nanorods (Fig. 4(a)) revealed the presence of Cu, In and O, which concurs with the XRD results (Fig. 1). The Ni and C in the spectra were assigned to the TEM grid. EDXS suggested that the CuO/In_2O_3 core–shell nanorods had been synthesized successfully by indicating a higher CuO concentration in the central region and a higher In_2O_3 concentration at both edge regions of the nanorod (Fig. 4(b)).

Fig. 5(a) shows the transient response of the pristine CuO nanorods and CuO/In_2O_3 core–shell nanorods, to C_2H_5OH at an operating temperature of 300 °C. The sensors were exposed to successive pulses of C_2H_5OH with concentrations ranging from 50 to 250 ppm. The response was reversible, i.e., the nanorod sensors showed the same resistance before and shortly after each ethanol pulse. Fig. 5(b) and (c) show an enlarged part of the data in Fig. 5(a) measured at a C_2H_5OH concentration of 250 ppm for the pristine CuO nanorods and CuO/In_2O_3 core–shell nanorods, respectively, to reveal the moments of gas input and gas stop. The pristine CuO nanorods showed responses of approximately 163, 192, 226, 242 and 291% at C_2H_5OH concentrations of 50, 100, 150, 200 and 250 ppm, respectively (Table 1). In contrast, the CuO/In_2O_3 core–shell nanorods showed responses of 382, 473, 618, 727 and 804% at C_2H_5OH concentrations of 50, 100, 150, 200 and 250 ppm, respectively (Table 1). The core–shell nanorod sensors showed ~2.3, 2.5, 2.7, 3.0 and 2.8 times higher responses than those of the pristine CuO nanorod sensors at C_2H_5OH concentrations of 50, 100, 150, 200 and 250 ppm, respectively (Table 1).

Fig. 5(d) shows the responses of the pristine CuO nanorods and CuO/In_2O_3 core–shell nanorods as a function of the C_2H_5OH concentration. The response of an oxide semiconductor is commonly expressed as $R=A[C]^n+B$, where A and B are constants, and n and [C] are the exponent and target gas concentration, respectively. Data fitting provided the following equations: $R=0.610[C]+132$ and $R=2.19[C]+271$ for the pristine CuO nanorod and CuO/In_2O_3 core–shell sensors, respectively. The response of the core–shell nanorod sensor increased more rapidly with increasing C_2H_5OH gas concentration than that of the pristine nanorod sensor. Although the response of the core–shell nanorods was examined only at C_2H_5OH concentrations of 50–250 ppm, the results suggest that the response of the former would be far higher than that of the latter at high C_2H_5OH gas concentrations such as a few thousand ppm of C_2H_5OH. On the other hand, the response and recovery times of the core–shell nanorods were similar to those of the pristine CuO nanorods.

Table 2 lists the responses of the CuO/In_2O_3 core–shell nanorod sensor fabricated in this study toward C_2H_5OH gas along with those of the other reported nanomaterial sensors. Overall, the sensing properties of the CuO/In_2O_3 core–shell nanorod sensor fabricated in this study were comparable to those of the other competing nanomaterials (Table 2) [32–46]. The C_2H_5OH concentration and test temperature used in this study were lower than those in previous studies. The response of the CuO/In_2O_3 core–shell nanorods was far higher than that of the TiO_2 nanotubes despite the far lower C_2H_5OH concentration and test temperature [32]. Compared to $CoFe_2O_4$ nanopowders, the CuO/In_2O_3 core–shell nanorods showed a somewhat lower response to C_2H_5OH gas and larger response and recovery times at the same temperature [39]. On the other hand, a comparison of the CuO/In_2O_3 core–shell nanorods with Co-doped ZnO nanorods measured at a similar C_2H_5OH concentration suggests that the response of the former was higher than that of the latter

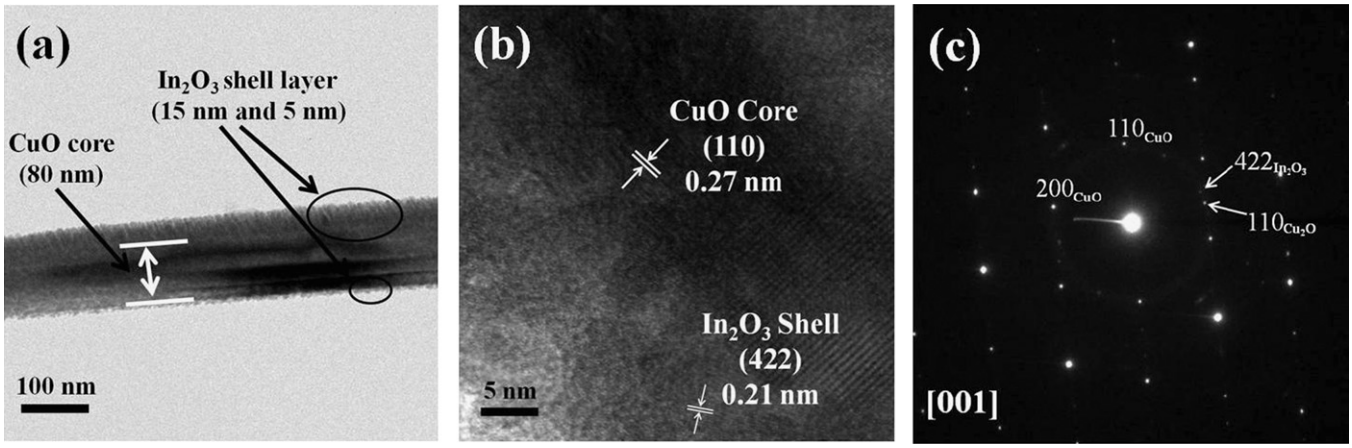

Fig. 3. (a) Low magnification TEM image, (b) high resolution TEM image, and (c) SAED pattern of CuO/In_2O_3 core–shell nanorods.

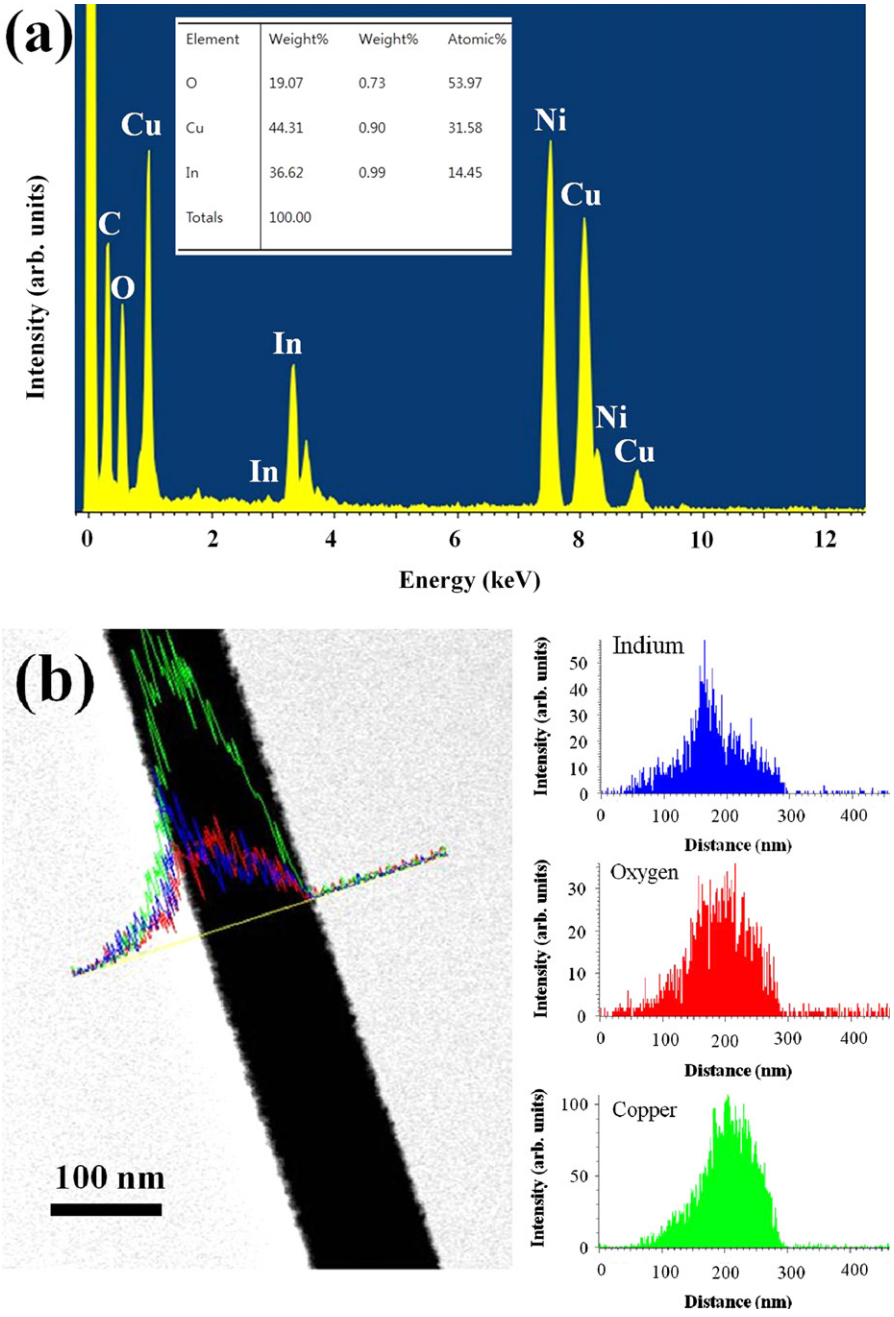

Fig. 4. (a) EDX spectrum of the CuO/In_2O_3 core–shell nanorods and (b) EDXS line scanning concentration profiles.

[40]. In particular, the response of the CuO/In_2O_3 core–shell nanorods is higher than that of plain In_2O_3 nanorods and nanocrystals despite the lower C_2H_5OH concentration.

CuO and In_2O_3 in the core–shell nanorods are p-type and n-type semiconductor oxides, respectively, and the sensing mechanism of the core–shell nanorods is based on a surface reaction. In this study, the CuO/In_2O_3 core-shell nanorods showed a considerably enhanced sensor response to ethanol gas. The surface of the sensor material is covered with chemisorbed oxygen ions such as O^-, O^{2-} and O_2^-, according to the following reactions [47]:

$$O_2(g) \rightarrow O_2(ads) \quad (3)$$

$$O_2(ads) + e^- \rightarrow O_2^-(ads) \quad (4)$$

$$O_2^-(ads) + e^- \rightarrow 2O^-(ads) \quad (5)$$

$$O^-(ads) + e^- \rightarrow O^{2-}(ads) \quad (6)$$

These adsorbed oxygen ions create a space charge region near the film surface by extracting electrons from the surface of the sensor. The adsorbed ethanol molecules react with these ionic oxygen species and produce electrons via the following two reactions: (Reaction 7) dehydrogenation of ethanol to an aldehyde and (Reaction 8) dehydration of ethanol to an alkene on basic and acidic oxides,

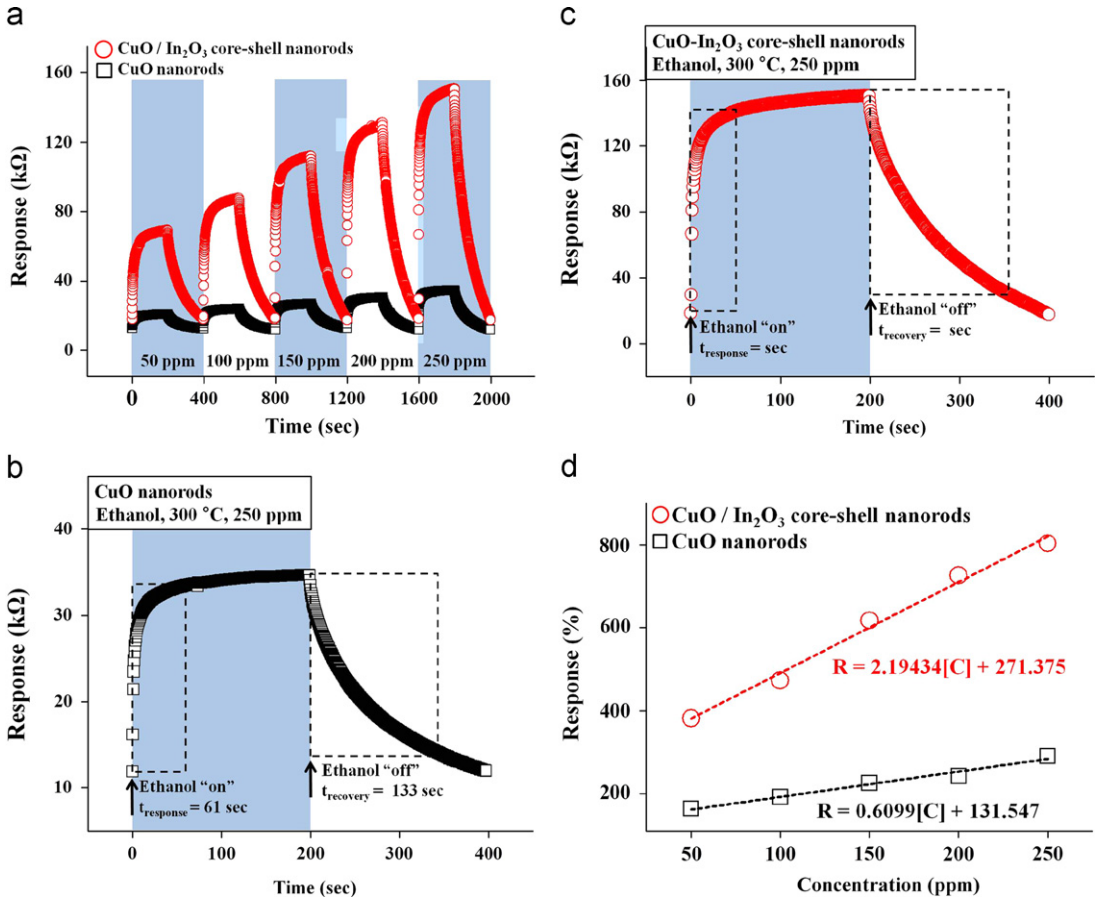

Fig. 5. (a) Dynamic responses of the pristine CuO nanorod and CuO/In_2O_3 core–shell nanorod gas sensors. (b) Enlarged part of (a) the pristine CuO nanorod at 250 ppm ethanol. (c) Enlarged part of (a) the core–shell nanorod at 250 ppm ethanol. (d) Responses of the pristine CuO nanorod gas sensors and the core–shell nanorod gas sensors as a function of the ethanol gas concentration.

Table 1
Responses, response times, and recovery times measured at different C_2H_5OH concentrations of the CuO/In_2O_3 core–shell nanorod sensor at 300 °C.

Ethanol conc.	Response (%)		Response time (s)		Recovery time (s)	
	CuO	CuO–In_2O_3	CuO	CuO–In_2O_3	CuO	CuO–In_2O_3
50ppm	163.66	381.77	61	53	133	149
100ppm	192.18	473.05	49	54	130	144
150ppm	225.95	617.64	39	40	140	154
200ppm	242.29	726.58	47	42	143	151
250ppm	291.08	803.59	31	36	142	153

respectively [48].

$$C_2H_5OH(g) \rightarrow CH_3CHO(g) + H_2(g) \quad (7)$$

$$C_2H_5OH(g) \rightarrow C_2H_4(g) + H_2O(g) \quad (8)$$

The enhanced sensor response of the CuO/In_2O_3 core–shell nanorods to ethanol compared to that of the pristine CuO nanorods might be due to the enhanced absorption and dehydrogenation of ethanol (Reaction 7) because of the basic properties of In_2O_3 [48,49]. The CH_3CHO is then oxidized by the chemisorbed oxygen ions according to the following equation:

$$CH_3CHO(ad) + 5O^- \rightarrow 2CO_2 + 2H_2O + 5e^- \quad (9)$$

In addition to the enhanced absorption and dehydrogenation of ethanol mentioned above, the enhanced response might be attributed partly to the modulation of electron transport by the In_2O_3–In_2O_3 homojunction at the interface of nanorods with an adjustable energy barrier height. An energy barrier exists at the In_2O_3–In_2O_3 homojunction formed at the crossing point of the two core–shell nanorods. Electron transport is modulated by the homojunction with an adjustable energy barrier height. Therefore, the homojunction acts as a lever in electron transfer through which electron transfer is facilitated or restrained, resulting in enhanced sensing properties of the nanorod sensor.

On the other hand, the enhanced sensor response of the core–shell nanorods might not be due to the changes in resistance due to CuO–In_2O_3 heterojunction barrier in each core–shell nanorod [50,51]. The width of the surface layer is in the order of the Debye length λ_D, which can be

Table 2
Comparison of the responses, response times and recovery times of the CuO/In_2O_3 core–shell nanorods (NR) sensor with those of other oxide 1D nanostructure sensors.

Nanomaterials	Ethanol conc. (ppm)	Temp. (°C)	Response (%)	Response time (s)	Recovery time (s)	Ref.
CuO/In_2O_3 nanorods	50	300	382	53	149	Present work
CuO/In_2O_3 nanorods	250	300	804	36	153	Present work
TiO_2 nanotubes	5000	200	16	–	–	32
SnO_2 nanorods	300	300	3140	1	1	33
Ce–SnO_2 nanopowders	200	250–450	18,500	–	–	34
Pt–SnO_2 nanopowders	100	150–350	4000	12	360	35
SnO_2–ZnO(0.05) composite nanopowders	300	200–400	390,000	96–418	400–600	36
ZnO–SnO_2(0.05) composite nanopowders	300	200–400	120,000	96–418	400–600	36
ZnO nanowires	1500	300	61	–	–	37
TiO_2 nanobelts	500	250	3366	1–2	1–2	38
Ag–TiO_2 nanobelt	500	200	4171	1–2	1–2	38
$CoFe_2O_4$ nanopowders	50	150	7190	50	60	39
Co–ZnO nanorods	50	350	987	–	–	40
In_2O_3 nanowires	100	370	200	10	20	41
In_2O_3 nanowires	100	275	240	–	–	42
In_2O_3 nanocrystals	69	270	270	–	–	43
In_2O_3 nanorods	50	–	795	5	10	44
In_2O_3 nanorods	50	330	11,500	6	11	45
In_2O_3 nanofibers	15,000	300	379,000	1	5	46

expressed as [52,53]

$$\lambda_D = \left(\varepsilon kT/q^2 n_c\right)^{1/2}, \quad (10)$$

where ε is the static dielectric constant ($8.9 \times 8.85 \times 10^{-12}$ F/m in In_2O_3), k is the Boltzmann constant (1.38×10^{-23} J/K), T is the absolute temperature (573 K), q is the electrical charge of the carrier (1.6×10^{-19} C) and n_c is the carrier concentration (9.5×10^{18} /cm^3: the value obtained by Hall measurements of a 200 nm In_2O_3 thin film deposited on a Si (100) substrate by sputtering). For the In_2O_3 layer on the core–shell nanorods fabricated in this study, the calculated λ_D value at 300 °C was approximately 1.6 nm. This means that C_2H_5OH molecules cannot donate/accept electrons to/from the CuO core but only to/from the In_2O_3 shell layer, the width of which is approximately 5–15 nm. Therefore, the heterojunction barrier at the interface of the core and shell does not need to be considered in this core–shell nanorod system.

4. Conclusions

CuO/In_2O_3 core–shell nanorods were synthesized using a two-step process: the synthesis of CuO nanorods using a thermal evaporation method and the subsequent deposition of In_2O_3. The cores and shells of the nanorods were single crystal CuO and polycrystalline In_2O_3, respectively. The responses of the CuO nanorods were improved approximately 2–3 fold at each C_2H_5OH concentration as a result of the sheathing with In_2O_3. The responses of the core–shell nanorods to C_2H_5OH gas were also far superior to those of the other material nanosensors reported previously. The improvement in the response of the CuO nanorods to C_2H_5OH gas by sheathing them with In_2O_3 might be due to the enhanced absorption and dehydrogenation of ethanol. In addition, the enhanced sensor response of the core–shell nanorods was attributed partly to changes in resistance due to the potential barriers built at the In_2O_3–In_2O_3 homojunction at the interface of the two nanorods.

Acknowledgment

This study was supported by Key Research Institute Program through the National Research Foundation of Korea (NRF) funded by the Ministry of Education, Science and Technology (2011-0018394).

References

[1] A.E. Rakhshani, Preparation, characteristics and photovoltaic properties of cuprous-oxide—a review, Solid-State Electronics 29 (1986) 7–17.
[2] B. Balamurugan, B.R. Mehta, Optical and structural properties of nanocrystalline copper oxide thin films prepared by activated reactive evaporation, Thin Solid Films 396 (2001) 90–96.
[3] K. Zhou, R. Wang, B. Xu, Y. Li, Synthesis, characterization and catalytic properties of CuO nanocrystals with various shapes, Nanotechnology 17 (2006) 3939–3943.
[4] L.B. Chen, N. Lu, C.M. Xu, H.C. Yu, T.H. Wang, Electrochemical performance of polycrystalline CuO nanowires as anode material for Li ion batteries, Electrochimica Acta 54 (2009) 4198–4201.
[5] Y.W. Zhu, T. Yu, F.C. Cheong, X.J. Xu, C.T. Lim, V.B.C. Tan, J.T.L. Thong, C.H. Sow, Large-scale synthesis and field emission properties of vertically oriented CuO nanowire films, Nanotechnology 16 (2005) 88–92.
[6] J. Zhang, J. Liu, Q. Peng, X. Wang, Y. Li, Nearly monodisperse Cu_2O and CuO nanospheres: preparation and applications for sensitive gas sensors, Chemistry of Materials 18 (2006) 867–871.

[7] A.H. MacDonald, Superconductivity—copper oxides get charged up, Nature 414 (2001) 409–410.
[8] H.M. Fan, L.T. Yang, W.S. Hua, X.F. Wu, Z.Y. Wu, S.S. Xie, B.S. Zou, Controlled synthesis of monodispersed CuO nanocrystals, Nanotechnology 15 (2004) 37–42.
[9] S.B. Wang, C.H. Hsiao, S.J. Chang, K.T. Lam, K.H. Wen, S.C. Hung, S.J. Young, B.R. Huang, A CuO nanowire infrared photodetector, Sensors and Actuators A 171 (2011) 207–211.
[10] C.T. Hsieh, J.M. Chen, H.H. Lin, H.C. Shih, Field emission from various CuO nanostructures, Applied Physics Letters 83 (2003) 3383–3385.
[11] A. Cruccolini, R. Narducci, R. Palombari, Gas absorption effect on surface conductivity of nonstoichiometric CuO, Sensors and Actuators B 98 (2004) 227–232.
[12] Y.S. Kim, I.S. Hwang, S.J. Kim, C.Y. Lee, J.H. Lee, CuO nanowire gas sensors for air quality control in automotive cabin, Sensors and Actuators B 135 (2008) 298–303.
[13] X. Gou, G. Wang, J. Yang, J. Park, D. Wexler, Chemical synthesis, characterization and gas sensing performance of copper oxide nanoribbons, Journal of Materials Chemistry 18 (2008) 965–969.
[14] J. Chen, K. Wang, L. Hartman, W. Zhou, H_2S detection by vertically aligned CuO nanowire array sensors, Journal of Physical Chemistry C 112 (2008) 16017–16021.
[15] C. Wang, X.Q. Fu, X.Y. Xue, Y.G. Wang, T. Hwang, Surface accumulation conduction controlled sensing characteristic of p-type CuO nanorods induced by oxygen adsorption, Nanotechnology 18 (2007) 145506–145510.
[16] L. Liao, Z. Zhang, B. Yan, Z. Zheng, Q.L. Bao, T. Wu, C.M. Li, Z.X. Shen, J.X. Zhang, H. Gong, J.C. Li, T. Yu, Multifunctional CuO nanowire devices: p-type field effect transistors and CO gas sensors, Nanotechnology 20 (2009) 085203–085208.
[17] Y. Chang, H.C. Zeng, Controlled synthesis and self-assembly of single crystalline CuO nanorods and nanoribbons, Crystal Growth and Design 4 (2004) 397–402.
[18] A.A. Umar, M. Oyama, A seed-mediated growth method for vertical array of single-crystalline CuO nanowires on surfaces, Crystal Growth and Design 7 (2007) 2404–2409.
[19] W. Wang, Y. Zhuang, L. Li, Structure and size effect of CuO nanowires prepared by low temperature solid-phase process, Materials Letters 62 (2008) 1724–1726.
[20] K. Zhang, C. Rossi, C. Tenailleau, P. Alphonse, J.Y. Chane-Ching, Synthesis of large-area and aligned copper oxide nanowires from copper thin film on silicon substrate, Nanotechnology 18 (2007) 275607–275614.
[21] P. Saravanan, S. Alam, G.N. Mathur, A liquid–liquid interface technique to form films of CuO nanowhiskers, Thin Solid Films 491 (2005) 168–172.
[22] C.M. Tsai, G.D. Chen, T.C. Tseng, C.Y. Lee, C.T. Huang, W.Y. Tsai, W.C. Yang, M.S. Yeh, T.R. Yew, CuO nanowire synthesis catalyzed by a CoWP nanofilter, Acta Materialia 57 (2009) 1570–1576.
[23] X. Jiang, T. Herricks, Y. Xia, CuO nanowires can be synthesized by heating copper substrates in air, Nano Letters 2 (2002) 1333–1338.
[24] A. Kolmakov, Y. Zhang, G. Cheng, M. Moskovits, Detection of CO and O_2 using tin oxide nanowire sensors, Advanced Materials 15 (2003) 997–1000.
[25] D.H. Zhang, Z.Q. Liu, C. Li, T. Tang, X.L. Liu, S. Han, B. Lei, C.W. Zhou, Detection of NO_2 down to ppb levels using individual and multiple In_2O_3 nanowire devices, Nano Letters 4 (2004) 1919–1924.
[26] H. Kim, C. Jin, S. Park, S. Kim, C. Lee, H_2S gas sensing properties of bare and Pd-functionalized CuO nanorods, Sensors and Actuators B 161 (2012) 594–599.
[27] X. Xue, L. Xing, Y. Chen, S. Shi, Y. Wang, T. Wang, Synthesis and H_2S sensing properties of $CuO-SnO_2$ core/shell pn-junction nanorods, Journal of Physical Chemistry C 112 (2008) 12157–12160.
[28] Y.J. Chen, C.L. Zhu, L.J. Wang, P. Cao, M.S. Cao, X.L. Shi, Synthesis and enhanced ethanol sensing characteristics of α-Fe_2O_3/SnO_2 core–shell nanorods, Nanotechnology 20 (2009) 045502–045507.
[29] J.Y. Park, S.W. Choi, J.W. Lee, C. Lee, S.S. Kim, Synthesis and gas sensing properties of TiO_2–ZnO core–shell nanofibers, Journal of the American Ceramic Society 92 (2009) 2551–2554.
[30] H.Y. Chen, Y.B. Chu, H.C. Shih, Phase transformations in copper oxide nanowires, Journal of Vacuum Science and Technology B 23 (2005) 2557–2560.
[31] C.H. Xu, C.H. Woo, S.Q. Shi, Formation of CuO nanowires on Cu foil, Chemical Physics Letters 399 (2004) 62–66.
[32] N. Kilinç, E. Sennik, Z.Z. Ozuturk, Fabrication of TiO_2 nanotubes by anodization of Ti thin films for VOC sensing, Thin Solid Films 520 (2011) 953–958.
[33] Y.J. Chen, X.Y. Xue, Y.G. Wang, T.H. Wang, Synthesis and ethanol sensing characteristics of single crystalline SnO_2 nanorods, Applied Physics Letters 87 (2005) 233503–2330505.
[34] F. Pourfayaz, Y. Mortazavi, A. Khodadadi, S. Ajami, Ceria-doped SnO_2 sensor highly selective to ethanol in humid air, Sensors and Actuators B 130 (2008) 625–629.
[35] G. Neri, A. Bonavita, G. Micali, N. Donato, F.A. Deorsola, P. Mossino, I. Amato, B. De Benedetti, Ethanol sensors based on Pt-doped tin oxide nanopowders synthesised by gel-combustion, Sensors and Actuators B 117 (2006) 196–204.
[36] S. Hemmati, A.A. Firooz, A.A. Khodadadi, Y. Mortazavi, Nanostructured SnO_2–ZnO sensors: highly sensitive and selective to ethanol, Sensors and Actuators B 160 (2011) 1298–1303.
[37] T.J. Hsueh, C.L. Hsu, S.J. Chang, I.C. Chen, Laterally grown ZnO nanowire ethanol gas sensors, Sensors and Actuators B 126 (2007) 473–477.
[38] P. Hu, G. Du, W. Zhou, J. Cui, J. Lin, H. Liu, D. Liu, J. Wang, S. Chen, Enhancement of ethanol vapor sensing of TiO_2 nanobelts by surface engineering, Applied Materials and Interfaces 2 (2010) 3263–3269.
[39] X. Chu, D. Jiang, Y. Guo, C. Zheng, Ethanol gas sensor based on $CoFe_2O_4$ nano-crystallines prepared by hydrothermal method, Sensors and Actuators B 120 (2006) 177–181.
[40] Y.J. Li, K.M. Li, C.Y. Wang, C.I. Kuo, L.J. Chen, Low-temperature electrodeposited Co-doped ZnO nanorods with enhanced ethanol and CO sensing properties, Sensors and Actuators B 161 (2012) 734–739.
[41] C. Xiangfeng, W. Caihong, J. Dongli, Z. Chenmou, Ethanol sensor based on indium oxide nanowires prepared by carbothermal reduction reaction, Chemical Physics Letters 399 (2004) 461–464.
[42] K. Ryu, D. Zhang, C. Zhou, High-performance metal oxide nanowire chemical sensors with integrated micromachined hotplates, Applied Physics Letters 92 (2008) 093111.
[43] W.H. Zhang, W.D. Zhang, L.Y. Chen, Highly sensitive detection of explosive triacetone triperoxide by an In_2O_3 sensor, Nanotechnology 21 (2010) 315502.
[44] J.Q. Xu, Y.P. Chen, Q.Y. Pan, Q. Xiang, Z.X. Cheng, X.W. Dong, A new route for preparing corundum-type In_2O_3 nanorods used as gas-sensing materials, Nanotechnology 18 (2007) 115615.
[45] J. Xu, Y. Chen, J. Shen, Ethanol sensor based on hexagonal indium oxide nanorods prepared by solvothermal methods, Materials Letters 62 (2008) 1363–1365.
[46] W. Zheng, X. Lu, W. Wang, Z. Li, H. Zhang, Y. Wang, Z. Wang, C. Wang, A highly sensitive and fast-responding sensor based on electrospun In_2O_3 nanofibers, Sensors and Actuators B: Chemical 142 (2009) 61–65.
[47] K.D. Schierbaum, U. Weimar, W. Gopel, R. Kowalkowski, Conductance, work function and catalytic activity of SnO_2-based gas sensors, Sensors and Actuators B 3 (1991) 205–214.
[48] T. Jinkawa, G. Sakai, J. Tamaki, N. Miura, N. Yamazoe, Relationship between ethanol gas sensitivity and surface catalytic property of tin oxide sensors modified with acidic or basic oxides, Journal of Molecular Catalysis A: Chemical 155 (2000) 193–200.
[49] K.W. Kim, P.S. Cho, S.J. Kim, J.H. Lee, C.Y. Kang, J.S. Kim, S.J. Yoon, The selective detection of C_2H_5OH using SnO_2–ZnO thin

film gas sensors prepared by combinatorial solution deposition, Sensors and Actuators B 123 (2007) 318–324.
[50] B.R. Huang, J.C. Lin, Core–shell structure of zinc oxide/indium oxide nanorod based hydrogen sensors, Sensors and Actuators B 174 (2012) 389–393.
[51] C. Xu, J. Tamaki, N. Miura, N. Yamazoe, Grain size effects on gas sensitivity of porous SnO_2-based elements, Sensors and Actuators B 3 (1991) 147–155.
[52] H. Ogawa, M. Nishikawa, A. Abe, Hall measurement studies and electrical conduction model of tin oxide ultrafine particle films, Journal of Applied Physics 53 (1982) 4448–4453.
[53] N. Barsan, U. Weimar, Conduction model of metal oxide gas sensors, Journal of Electroceramics 7 (2001) 143–167.